Distribution Agreement

In presenting this thesis as a partial fulfillment of the requirements for a degree from Emory University, I hereby grant to Emory University and its agents the non-exclusive license to archive, make accessible, and display my thesis in whole or in part in all forms of media, now or hereafter now, including display on the World Wide Web. I understand that I may select some access restrictions as part of the online submission of this thesis. I retain all ownership rights to the copyright of the thesis. I also retain the right to use in future works (such as articles or books) all or part of this thesis.

Jiatian Wu May 9, 2020

Optical Spectroscopy of Moiré Structures: Light-Induced Effective Magnetic Field in Atomic Thin Materials

By

Jiatian Wu

Ajit Srivastava

Adviser

Department of Physics

Ajit Srivastava

Adviser

Hayk Harutyunyan

Committee Member

Michael Rogers

Committee Member

2020

Optical Spectroscopy of Moiré Structures: Light-Induced Effective Magnetic Field in Atomic Thin Materials

By

Jiatian Wu

Ajit Srivastava

Adviser

An abstract of
a thesis submitted to the Faculty of Emory College of Arts and Sciences
of Emory University in partial fulfillment
of the requirements of the degree of
Bachelor of Science with Honors

Department of Physics

2020

Abstract

Optical Spectroscopy of Moiré Structures: Light-Induced Effective Magnetic Field in Atomic Thin Materials

By Jiatian Wu

When atomic thin materials (ATMs) are brought together with a small twist angle, the heterobilayer system gives rise to some new optical and magnetic properties, such as moiré excitons and emergent many-body phases [1, 2, 3, 4, 5]. Due to Coulomb interaction between the electrons and holes in a semiconductor, they are bound as pairs named excitons and determine the optical response such as light absorption and emission. Our lab focuses on the study of transition metal dichalcogenides (TMDs) such as $MoSe_2$ and WSe_2, which are unique in a way that their charge carriers possess a "valley" degree of freedom which acts like a pseudo spin and can be controlled by helicity of light. The valley-dependent optical selection rules allow us to manipulate the valley degree of freedom and investigate exciton interactions through light polarization techniques. Our group has previously shown a repulsive dipole-dipole interaction between excitons [6], and now we report an additional exciton exchange interaction within the same valley species. Moreover, we find that the exchange interaction induces a magnetic-field-like effect, which can be manipulated by optical pumping. The finding of the optical-induced splitting provides another knob to control the valley degree of freedom and can be applied to future "valleytronics" applications, in which information is stored and processed in the valley degree of charge carriers.

Optical Spectroscopy of Moiré Structures: Light-Induced Effective Magnetic Field in Atomic Thin Materials

By

Jiatian Wu

Ajit Srivastava

Adviser

A thesis submitted to the Faculty of Emory College of Arts and Sciences
of Emory University in partial fulfillment
of the requirements of the degree of
Bachelor of Science with Honors

Department of Physics

2020

Acknowledgements

First, I would like to thank Prof. Hayk Harutyunyan and Prof. Michael Rogers for taking their time to serve on my committee. I would also like to thank Prof. Ajit Srivastava for having me in his group and providing me his wisdom and guidance through my thesis research. My genuine thanks also go to Dr. Xin Lu and Weijie Li for their kind support and encouragements throughout the project, without which I would not have made it through!

Contents

1 Introduction

1.1 Atomic Thin Materials

The discovery of atomic-thin graphene is significant in many ways, for not only being the first two-dimensional (2D) materials in existence but also spurring the growth in a variety of unconventional physics fields. Like many other historical discoveries in physics, the finding of graphene was rather accidental as the two physicists, Andre Geim and Konstantin Novoselov, used adhesive tapes to peel off layers from a graphite bulk repeatedly until its dimension was reduced to only a few atomic thick [7]. The mechanical exfoliation is possible due to the weak van der Waals interaction between crystal layers. Graphene is unique in a way that it presents exotic electronic and quantum properties owing to graphene's crystalline structure, such as massless electrons. Likewise, a range of materials with X-M-X structural properties (M=Mo, W; X=S, Se, shown in Fig.1a), or transition metal dichalcogenides (TMDs), are also layered similar to graphene, and exhibit a variety of electronic properties from semiconduction to supercondcuvitiy.

Similar to graphene, atomic thin TMD materials are easy to fabricate in a two-dimensional manner using the scotch-tape method, and some TMDs can be reduced to a single atomic thin structure. The monolayer TMDs have the honeycomb lattice structure with one M atom surrounded with three X atoms, as shown in Fig. 1a. Correspondingly, the reciprocal lattice of TMDs has the same hexagonal shape in the Brillouin zone after the Fourier transform of real space lattice. The symmetry of the reciprocal lattice is broken as each M atom in TMDs has inversely oriented neighboring X atoms. The inversion symmetry causes the K points with different directions to become inequivalent and be grouped into K and -K points, namely. The K (or -K) points correspond to the bandgap with the lowest energy state, which results in low energy physics taking place in the vicinity of K points (or K valleys) with opposite valley index.

It is worth mentioning that the main difference between graphene and TMD materials is their bandgaps. Unlike graphene with a zero bandgap, monolayer TMD materials have direct bandgap at K points in the range of visible or near-infrared light, making TMD materials a fitting platform for optical and electronic studies [8]. The direct bandgap of monolayer materials refers to the energy difference between the valance band maxima and the conduction band minima at the K-point. The semiconducting TMDs have a fully-occupied valance band and a fully-emptied conduction band separated by its bandgap. An electron requires a minimum amount of energy equivalent to the material's bandgap energy E_g to transit from the valence band to the conduction band, and thus the conductivity of TMD semiconductors is strongly dependent on its bandgap. When measuring TMD materials in a near-zero Kelvin environment, the materials are sensitive to light carried with photons, and electrons in the valence band respond accordingly to its bandgap energy.

The interband transition of electrons creates electron-hole pairs (or excitons) bounded by strong Coulomb interaction due to reduced screening [9]. Holes are created by the nature of lacking electrons. When an electron is excited to the conduction band, it leaves the valence band an absent spot with a positive charge known as a hole. An exciton consists of a negatively charged electron and a positively charged hole, which is analogous to a hydrogen atom with a 1 to 2 nm Bohr radius. Since exciton's Bohr radius is larger than TMDs' lattice constant, it allows monolayer excitons to move freely as pairs in between several unit cells, which indicates that the exciton dispersion is confined within a narrow range around K point in the momentum space. The neutral excitons X^0 in the monolayer have binding energy 0.32 - 0.86 eV, while electron-doped excitons X^- and hole-doped excitons X^+ have additional charging energy of 18-40 meV [10]. Thus, when pumping the material with lasers, it absorbs energy larger than the bandgap to form excitons and emit lower energy after electrons and holes recombine. The process is known as photoluminescence (PL), and 2D material studies utilize the PL technique to study the electronic properties of semiconducting TMD materials.

1.2 Optical Properties of TMDs

As mentioned above, semiconducting TMDs are sensitivity to light and thus serve as great photon emitters for optical measurements. At the meantime, inversion symmetry breaking in 2D TMD materials gives rise to possible manipulations of valley contrasting physics. These 2D TMD characteristics allow experiments to control valley polarization and explore electronic valley degrees of freedom using optical technique.

When we probe the material with circular polarized light, excitons have the tendency to stay in one valley species than the other species. The valley-dependent selection rule works as follows, the excitons in K (-K) valley with spin-up (spin down) couple to $\sigma+$ ($\sigma-$) circular polarized light correspondingly. The process involves two types of couplings, the spin-valley coupling and valley polarization coupling.

Theoretically, we can consider a simple band model of monolayer TMD material such as WSe_2. The band edges at the K point is dominated by the d-orbitals in the W atom, and its two-band Hamiltonian is

$$\hat{H} = at(\tau_z k_x \hat{\sigma}_x + k_y \hat{\sigma}_y) + \frac{\Delta}{2}\hat{\sigma}_z - \lambda\tau\frac{\hat{\sigma}_z - 1}{2}\hat{s}_z,$$

where the valley index $\tau_z = \pm 1$, a is the lattice constant, t is the effective hopping integral, Δ is the energy gap, and $\hat{\sigma}_y$ and $\hat{\sigma}_x$ are the Pauli matrix basis of two d-orbitals with magnetic moments m = 0 and m = $2\tau_z$. The last term in the above equation is contributed by the spin-orbital coupling (SOC) from the metal atom W in which 2λ is the spin splitting in the valence band due to SOC and $\hat{s}_z$ is the spin Pauli matrix [11]. The valence band edge has two d-orbitals ($d_{x^2+y^2}$ and d_{xy}), of which the degenerate state splits into spin-up and spin-down if taken SOC into account, whereas the conduction band with one d_{z^2} d-orbitals remains negligibly degenerate (illustrated in Fig.1c). Since the valence band has a large spin splitting in one valley, flipping of the spin index requires a relatively large magnetic energy; meanwhile, flipping of the valley index requires energy of atomic scale scattering. In

other words, spin and valley are locked in the valence band in the absence of such energy scatterings. For example, when excitons in K valley are excited, the hole-spin states in the valence band also get excited and maintain at its lowest energy state after relaxation (i.e., spin-up state).

In addition to the spin-valley coupling discussed above, we now focus on the causation of the coupling between valley and light helicity. The interband transition of an electron requires photon energy equivalent to splitting from the uppermost valence band to lowermost conduction band as recalled, and it is found that the coupling strength or probability of circular polarization is given as a function of wavevector k,

$$|\mathcal{P}_{\pm}(k)|^2 = \frac{m_0^2 a^2 t^2}{\hbar^2}(1 \pm \tau_z \frac{\Delta'}{\sqrt{\Delta'^2 + 4a^2t^2k^2}})^2,$$

where the interband transition Δ' is much larger than atk [11]. The equation shows that the valley excitation and emission are dependent on the helicity of light. Specifically, when pumping with $\sigma+$ circular polarized light, the electrons in the K valley get excited and emit light information encoded with $\sigma+$ polarization as well. Thus, we can use the valley-dependent selection rule to create excitons in either or both valley species by circular or linear polarized light. It is noted that the spin is conserved during the valley polarization process, and thus valley selection rule may as well become the spin selection rule as the valley, spin, and light polarization are conserved simultaneously.

1.3 Moiré Superlattice

Exotic physics properties such as superconductivity can be achieved in moiré structured graphene [15], and we would like to explore novel optical features in the 2D TMD system as well.

A large-scale moiré pattern emerges owning to the interference on the original repetitive patterns with small periods. A moiré superlattice can be formed by stacking two TMD layers

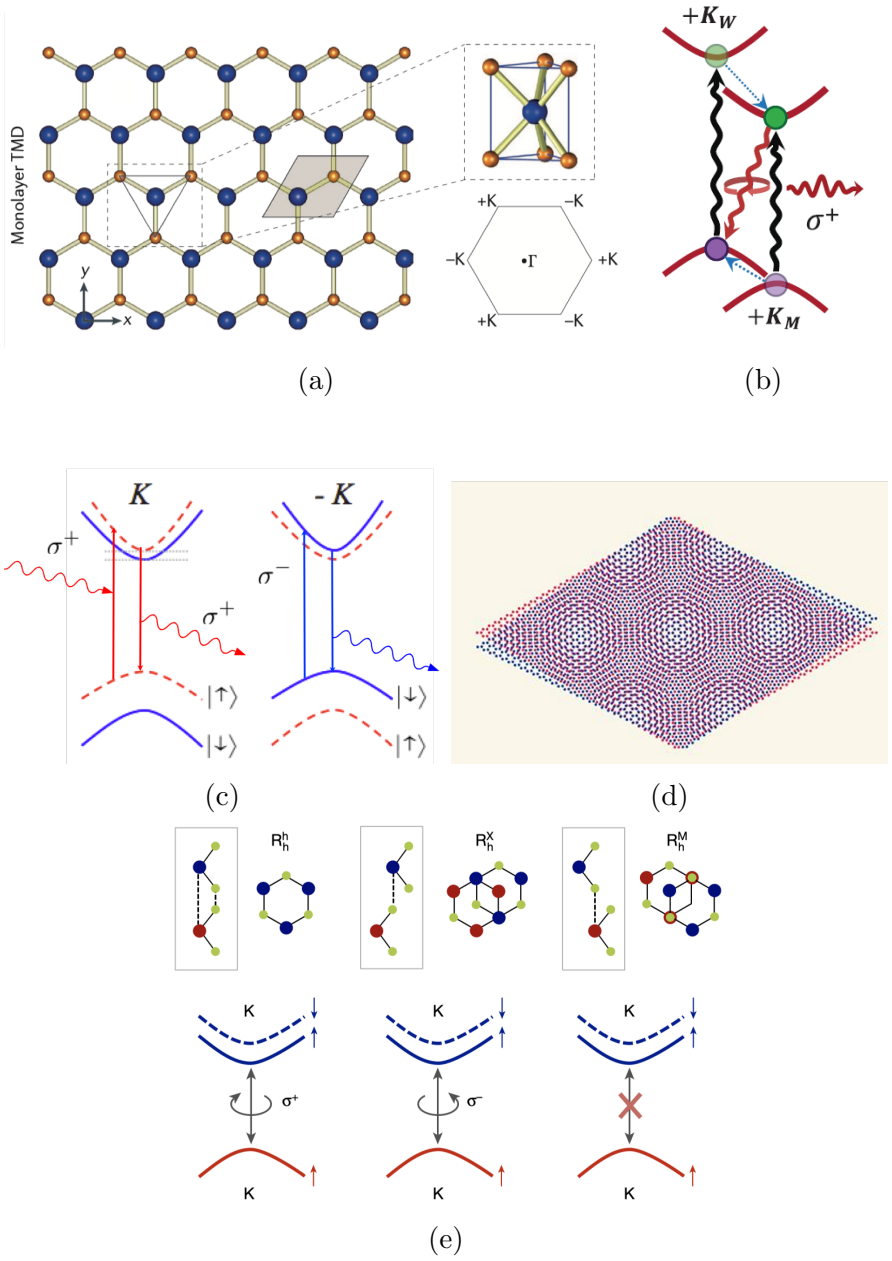

Figure 1: TMD materials. **a**. Monolayer TMD crystalline structure. Figure adopted from Ref.[12]. **b**. Type II band structure in $WSe_2/MoSe_2$. Figure adopted from Ref. [13]. **c**. Valley-dependent selection rule. **d**. Moiré structures in ATMs [14]. **e**. Three-fold symmetry in moiré TMD and the optical selection rule [1].

together with a small twisted angle (shown in Fig.1d), and the deep moiré potentials also appear to localize excitons when its superlattice has a 10nm or larger period [16]. There are two types of high symmetry configurations in stacking TMD materials, the R-type and the H-type stacking. The formation of moiré superlattice preserves the three-fold symmetry as in the hexagonal TMD lattice - meaning that the moiré supercell has three symmetric points at the local energy extrema, denoted as R_h^h, R_h^X, R_h^M registries in R-type for example (shown in Fig.1e).

Structural changes from monolayer to moiré lattice also affects the optical nature of the TMD materials, and the spatial factor has also to be taken into account for the optical selection rules for the moiré valleys. The valley polarization still applies to the moiré structured materials, but the relative position of M- and X- atoms also matters in this case. In Fig.1e, it shows that the polarized light only couples to excitons localized at R_h^h, R_h^X and light emission is forbidden at R_h^M registration [1].

Moreover, the magnetic field in moiré superlattice tells important structural information about moiré twist angle. When an external magnetic field applies to the moiré sample, the energy between the conduction band and valence band shifts due to three factors, which are spin ($\Delta_s = 2s_z\mu_B B$), atomic orbital($\Delta_a = l_i\mu_B B$), and a valley ($\Delta_v = \tau a_i \mu_B B$) contribution to the energy splitting [17, 18, 19]. The variable τ is the valley index, s_z is the spin index, μ_B is the magnetic moment, and a_i is the g-factor of the conduction band (a_c, i=c) or valance band (a_v, i=v). The energy shift is namely the Zeeman effect, which will be discussed shortly. However, the former two factors are irrelevant to twist angle structure, and the energy shift contributed by the twist angle is only dealt with the valley pairing factor. At near zero degree twist angle, the interlayer exciton configuration lies both in K or -K valley, leading to energy splitting $\Delta 0^\circ = -2(2 - \Delta a)\mu_B B$; at near 60 degrees, the exciton lies in the opposite $K_W/-K_M$ or $-K_W/K_M$) valleys, leading to energy splitting $\Delta 60^\circ = -2(2 + \sum a)\mu_B B$. Here, Δa and $\sum a$ is the difference and summation of a_v and a_c. It is shown experimentally by Xu's group that the moiré sample with g-factor of 6.7 and -15.9 corresponds to 0° and

60° twist angle [2].

1.4 State of a Two-Spin System

We have discussed about the optical interactions of the monolayer system in the light of Coulomb interaction, and similar physics applies to the heterolayer structure as well, which provides a new angle of view to understand the optical physics in many-body states system. In specific, we study the optical and electronic effects in the heterobilayer system of $WSe_2/MoSe_2$. The $WSe_2/MoSe_2$ heterobilayer forms a type-II band structure (shown in Fig. 1b), and the exciton is found to stay in a stable, long-lived state between the heterobilayers by its structural nature [20]. The interlayer exciton behaves like an electric dipole with fixed orientation of which the electrons live in $MoSe_2$ layer and the holes live in WSe_2 layer [13]. In addition, repulsive dipolar interaction should take place in the presence of many-body interlayer excitons, and previous studies have demonstrated the dipole-dipole interaction U_{dd} in the heterolayer system. The studies show that the creation of the second interlayer exciton $|IXX\rangle$ within a potential well requires an extra on-site energy cost U_{dd} other than the single excitation energy E_x for the first interlayer exciton $|IX\rangle$ caused by diploar interaction, shown in Fig.2a [6].

While dipole-dipole interaction has been observed, exchange interaction should also be taken into consideration in the many-body exciton analysis. The exchange interaction is a result of indistinguishable particles in the quantum mechanical sense. Excitons are boson particles of which the states are symmetric under interchange. The complete wave function of a two-exciton state $\psi(r)\chi$ consists both the spatial $\psi(r_1, r_2)$ and spin part, $\chi(1, 2)$, which can be both anti-symmetric or symmetric to maintain the total symmetry. In the anti-symmetric case, the two spins forms an anti-symmetric singlet configuration, and the anti-symmetric spatial function indicates the two dipoles staying farther apart; on the contrary, the symmetric case forms the triple configuration, and the dipoles tend to overlap on each other resulting from the spatial wave function symmetry, resulting a larger dipolar repulsion

U_{dd}. The latter case generates larger exchange interaction energy U_{ex} than the former case, given the quantum mechanical phenomenon of indistinguishability.

Therefore, since the excitons in one valley species always have the same spins due to the spin-valley locking effect, there is an additional exchange energy to be considered when the excitons are created in the same valley with the same spins. In other words, the valley of which more excitons are created should have larger exchange energy and thus increasing energy band gap than the other valley (shown in Fig.2b). Experimentally, when the sample is excited with linearly polarized light, both valley species are created equally; when the sample is probed by circular polarized light, one valley species have larger density than the other, which results the imbalance between valley species.

1.5 Zeeman-like Splitting

We discussed in the previous section that the interlayer excitons should have exchange interaction in the same valley or spin, resulting in a change of the corresponding energy band (as illustrated in Fig.2b. Interestingly, a similar energy shift can be achieved in the magnetic field caused by the valley Zeeman effect [18].

The inversion symmetry breaking is the underlying cause of Zeeman splitting. In the limit of 2D materials, the orbital currents can only circulate in the plan, leading its magnetic moment to only point out-of-plane. Since the charge particles in K and -K valleys possess opposite magnetic moments, the applied magnetic field should have opposite effects in the two valley species. The energy shift in each valley species is $-\mu B$, and thus we can lift the valley degeneracy by applying B field to both K and -K valleys.

Now that by utilizing the spin-valley locking property and optical spectroscopy technique, we can observe the energy/wavelength difference in the $\sigma\pm$ emission spectra, we can observe the Zeeman splitting effect in B field measurements. On the other hand, if the excitons have exchange interaction within one valley as we predict, the valley degeneracy can be lifted by optical pumping as well and perform a similar energy splitting effect like Zeeman splitting

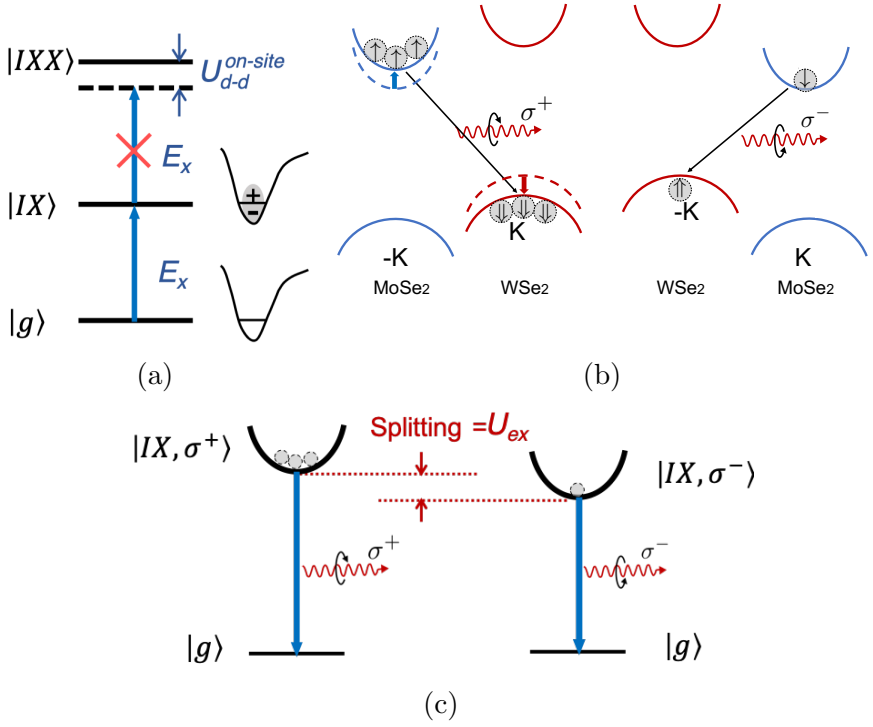

Figure 2: Interlayer excitons dipole interactions. **a**. Dipole-dipole interaction. Figure adopted from Ref.[6]. **b**. Exciton-exciton exchange interaction. **c**. Band structure of exchange interaction.

does under B field.

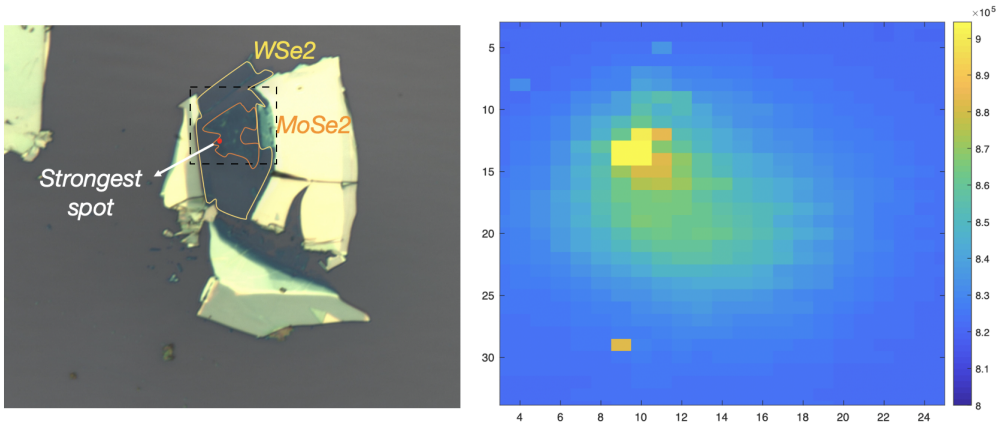

(a) (b)

Figure 3: Heterobilayer Sample **a**. An optical image of WSe_2 /$MoSe_2$ heterobilayer sample. Monolayer WSe_2($MoSe_2$) is depicted in yellow (orange) solid line. The red dot is the spot with the highest PL signal. **b**. A PL scan of the sample. The x,y axis represents the steps taken for the scanning. The black dashed line in the left figure is the approximate PL scan range.

2 Methods

2.1 Sample Fabrication

Sample preparation remains a key step for good PL measurements. We obtain the WSe_2 and $MoSe_2$ monolayers by mechanical exfoliation. The two monolayers are then transferred to a 300 nm SiO_2/Si substrate, with WSe_2 at the bottom and $MoSe_2$ at the top. WSe_2 and $MoSe_2$ are stacked together as their top-left edges are parallelly aligned, shown in Fig.(3a). The twisted angle between the two layers is around 60°, which is verified in the g-factor measurement later. The sample is annealed in 5% H_2/95% N_2 at 125 °C for 2 hours.

2.2 Photoluminescence Spectroscopy

The heterobilayer sample is first loaded into closed-cycle cryostat (AttoDry 800) for PL measurements and then into another cryostat (BlueFors cryogenics) for magnetic-field dependence test from -7 to 7 T. Both measurements are conducted at around 4 Kelvin in closed

vacuum chambers. A tunable continuous-wave Ti:Sapphire laser is used for excitation, and the laser spot size is around 1μm. The emission from the sample is collected by an achromatic lens and then goes to a high-resolution spectrometer with 300 grating/mm and 1200 grating/mm.

Before the sample gets excited, the laser goes through a series of optical lens and filters. A bandpass filter is put after the laser source, allowing only a certain range of light wavelength to pass through. The laser then go through the polarization control system to allow polarization degree of freedom manipulation. For example, the unpolarized laser has to go through a polarizer and a $\lambda/4$ waveplate to become circular polarized light. A beamsplitter is placed for changing the light path.

After the sample emission, the signals go through another set of polarization control system to provide the polarization detection degree of freedom. Take the circular excited and circular collected experiment as an example. The sample emits circular polarized light due to valley polarization, and the emission then is converted to linear polarized light through a $\lambda/4$ waveplate. The linearly polarized light is the superposition of left-handed ($\sigma-$) and right-handed ($\sigma+$) axis components, and a polarizer is placed after to allow only the light of one axis to pass through. The $\sigma\pm$ signals are collected in a spectrometer at the end.

In magnetic field measurements, the external B field is applied perpendicular to the plane of the sample. A schematics diagram of the optical measurement setup is shown in Fig.(4).

The emissions are recorded as spectrum data via LightField®, and Fig.(7) is a demonstration of the emission data we collect during measurements. The intensity, energy(or wavelength), and polarization are collected and analyzed. The intensity is the pixel counts of a certain wavelength value in the emission; the wavelength is the emission energy, which is converted by $E = hc/\lambda$; and the polarization is characterized by a parameter, degree of circular polarization (DCP), which is defined as

$$DCP = \frac{I(\sigma+) - I(\sigma-)}{I(\sigma+) + I(\sigma-)}, \tag{1}$$

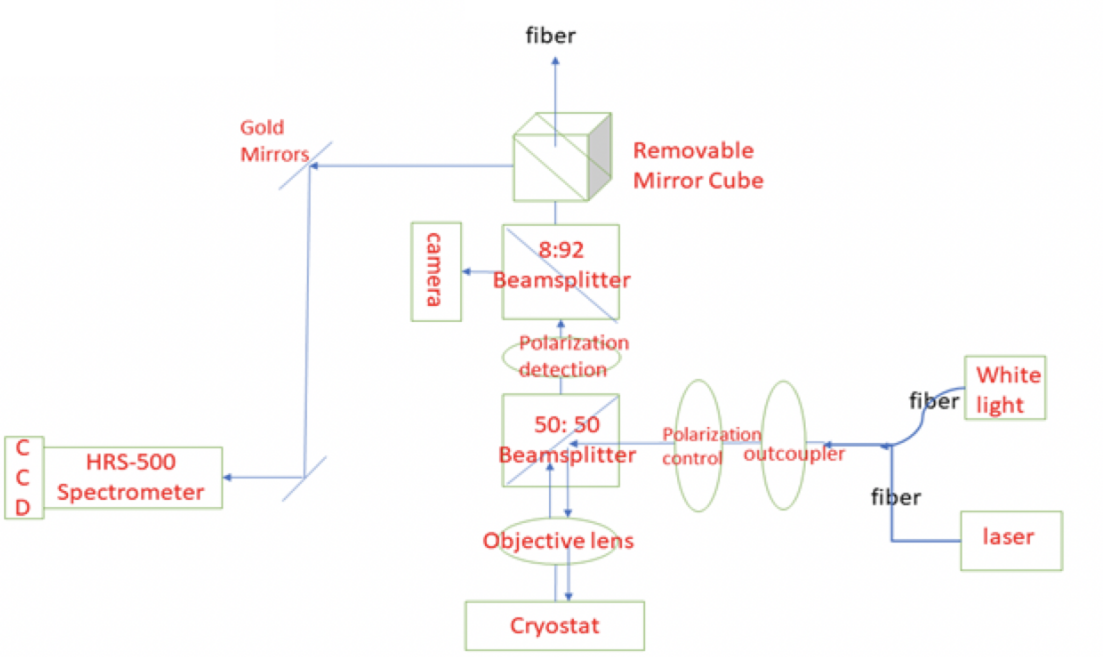

Figure 4: Setup Diagram.

where I is the intensity of one circular polarized species. To increase the precision of energy/wavelength peak, the data is imported to a numerical analysis software Igor Pro for curve fitting analysis.

3 Results and Discussion

A heterobilayer $WSe_2/MoSe_2$ sample is fabricated to show the exciton-exction exchange interaction U_{ex} in the limit of atomic thin materials. In particular, we would like to confirm the optical-induced effect of the pseudo B-field splitting under B field.

3.1 Zero Magnetic Field Measurements

The heterobilayer sample should create interlayer electron-hole pairs when probed by a tunable laser with a wavelength range. As Fig. 5a shows, the sample shows a prominent redshift of PL peak centered at 887nm, indicating the signal of which is localized interlayer excitons [21]. Next, the photoluminescence excitation spectroscopy (PLE) measurement is conducted to check the sample's response excited by the laser light from lower energy to higher energy. Fig.5b is the normalized intensity of the total reflection spectrum at the wavelength from 701nm to 778nm. The results in Fig. 5b, 5c show that the sample excitation resonates at 720nm and 755nm, which corresponds to WSe_2 and $MoSe_2$ intralayer exciton [22]. The PL and PLE measurements confirm that the excitons are first created within one layer and then become interlayer excitons after scattering to the other layer.

Next, we would like to confirm if the exciton imbalance exists between two valley species. As discussed before, valley polarization should cause a density imbalance between K and -K valley, dependent on the degree of circular polarization (DCP). Fig.6 is plotted by applying Eq. (1), which compares the intensity difference of X+ and X- excitons. Here, X+ represents the $\sigma+$ polarized exciton in the K valley, and X- the $\sigma-$ polarized exciton in the -K valley. When the sample is excited with circular polarized ($\sigma\pm$) light, the coupled valley species (K$\pm$) should be excited. As a side note, the other valley species (K$\mp$) can also be excited due to the scattering process but with much less density, and the overall excited excitons (X$\pm$) should be in consistent with valley polarization. Here, the figure shows that the exciton density has a drastic imbalance at 720nm excitation but no imbalance at 755nm excitation.

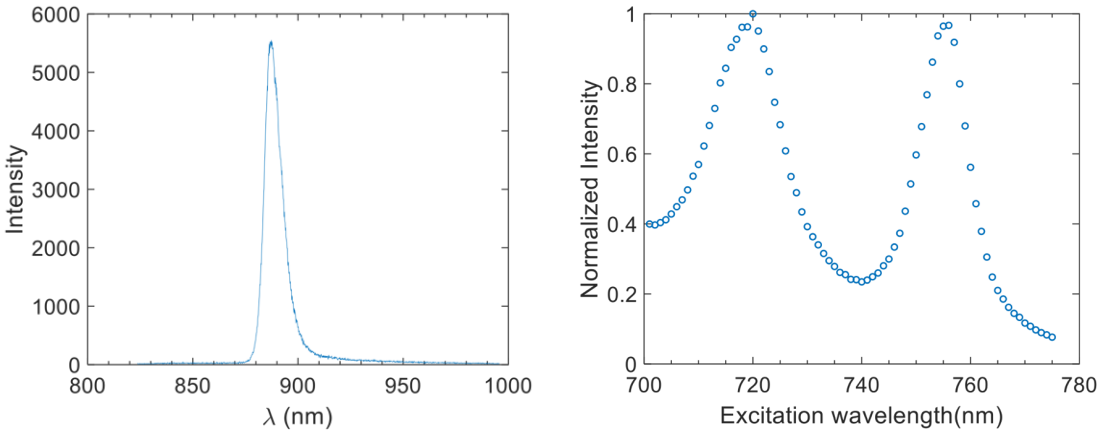

(a) (b)

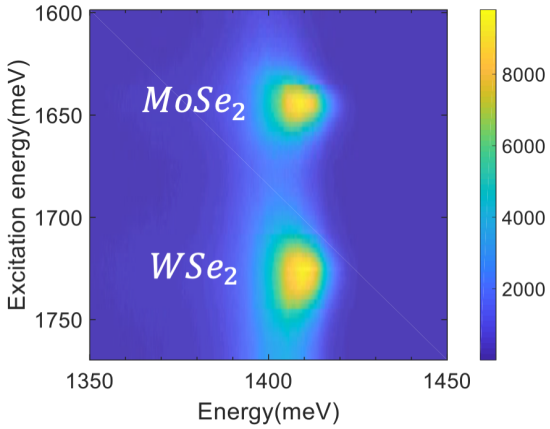

(c)

Figure 5: Photoluminescence excitation (PLE) test of interlayer excitons. The measurements are done in 1s using the TiS laser, excited in a range from 701 to 755nm wavelength. **a**. PL of interlayer excitons (∼900nm) at 4K with linearly polarized incident excitation and linear polarization collection. **b**. The normalized intensity of interlayer excitons dependent on excitation wavelength. The sample excites the most with 720nm and 755nm laser, which corresponds to WSe_2 and $MoSe_2$ resonances. **c**. The color plot of interlayer exciton PLE. The color bar is the intensity counts at a certain excited wavelength. It shows that interlayer excitons get excited at WSe_2 and $MoSe_2$ resonances. Fig.b can be treated as a horizontal cross section of the Fig.c.

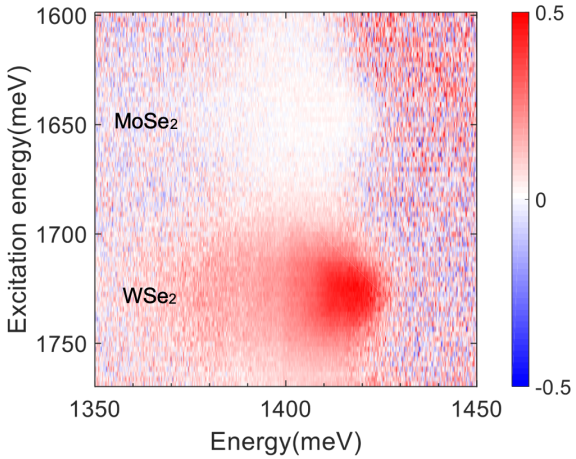

Figure 6: The color plot of DCP under circular excitation and circular collection. The color bar shows the sample's circular dichroism (CD). The interlayer excitons show a strong CD (= 0.5) at WSe_2(or 720nm) excitation, but no CDs at $MoSe_2$(or 755nm) excitation.

It is clear that the imbalance can be created at WSe_2 resonance but not $MoSe_2$, which aligns with previous studies [23].

Now that the imbalance due to valley polarization is confirmed, we proceed to investigate the effects caused by such imbalance from a energy level perspective. Interlayer excitons behave like electric dipoles with internal spins. An interesting scenairo occurs when excitons with the same spin states are excited in the same valley species: not only do excitons repels each other due to Coulomb interaction, they now also obtain exchange interaction with each other. Therefore, if the polarized-resolved measurements would create an density imbalance in valley species, we can deduce that the exchange interaction leads to an energy increase in one valley species than the other, resulting a splitting in the polarized-resolved PL spectrum. It is evident that the splitting in Fig.7 is caused by exchange interaction as the co-polarized emission curves under both $\sigma\pm$ polarized excitations have higher energy peak than the cross-polarized.

To verify our findings, a power dependence test is conducted to check if the splitting increases as more excitons are created. Indeed, we see a continuous increase in splitting as shown in Fig.8b. Initially, the splitting is negligible when the power pumping is small, and it increases up to 4meV with more power pumping. The splitting increase is caused by

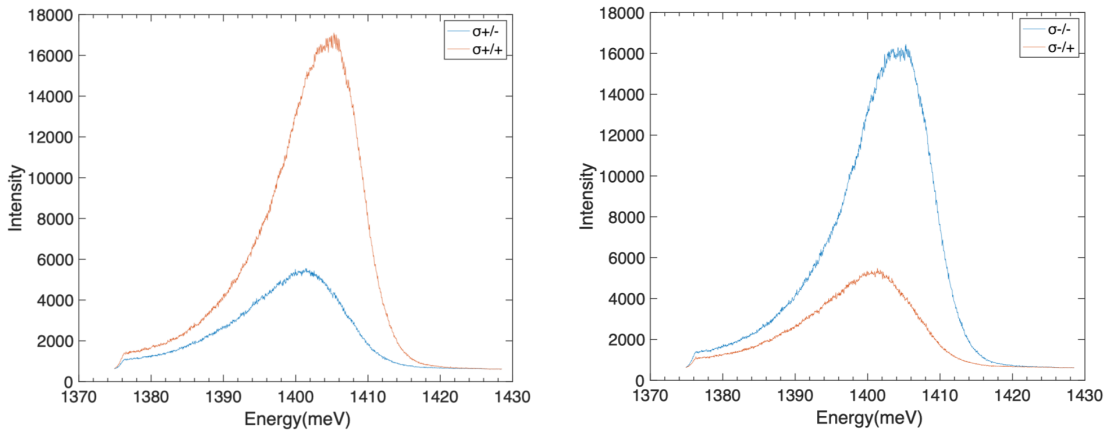

(a) (b)

Figure 7: Polarization resolved spectra. PL under $\sigma\pm$ excitation and circular basis($\sigma\pm$) collection . The co-polarized case is $\sigma+/\sigma+$ or $\sigma-/\sigma-$ with higher energy; and the cross-polarized case is $\sigma+/\sigma-$ or $\sigma-/\sigma+$ with lower energy.

exchange interactions in result of more X+ (or X-) creations in one valley species. Fig.8a proves that the splitting is caused by imbalance only, since a large splitting shows at 720nm excitation whereas the splitting at 755nm excitation is negligible.

The results are exciting as a pseudo-magnetic-field effect occurs in the sample by optical pumping. Without applying external B field, we are able to break the time-reversal symmetry by circular polarization and achieve a Zeeman-like splitting such that the energy of spins in K and -K valleys are separated in the momentum space.

3.2 Magnetic Field measurements

To further confirm our theory that an optical-induced B field is created, its splitting effect should be modulated by applying an external B field. If the optical-induced effect resembles the actual B field, the total splitting should be affected by both the density imbalance and the actual Zeeman splitting. Hence, we conduct experiments under B field to test whether the splitting caused by valley polarization is effectively enhanced or cancelled.

First of all, a comparison test is conducted to confirm that valley polarization is the direct causation of the previous Zeeman-like splitting. The sample is excited with linearly-polarized

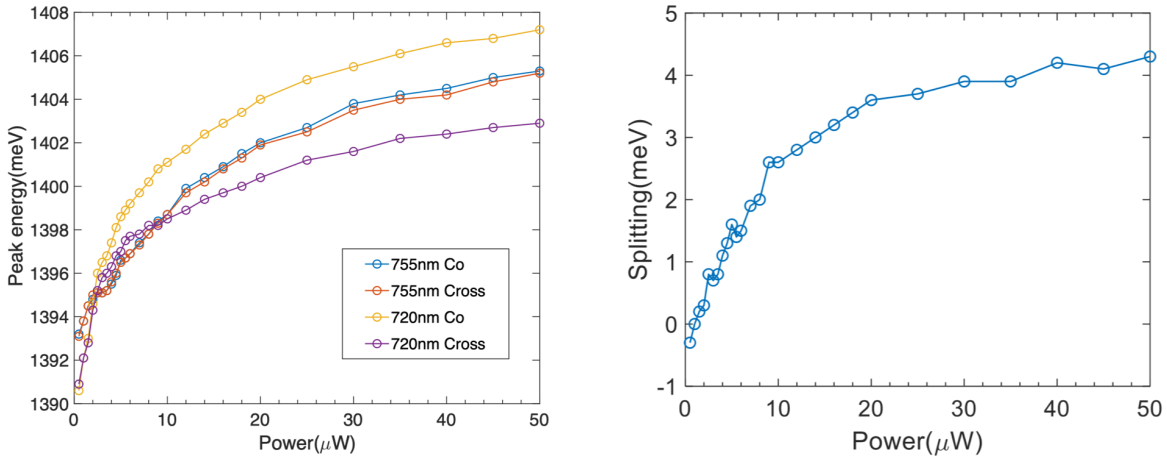

(a) (b)

Figure 8: Power dependence test under circular excitation and circular collection. **a**. The peak energy with co-polarization and cross-polarization dependent on power. The sample is excited with 720nm TiS laser for 5s each. **b**. The power dependent energy splitting with 720nm excitation at 0T.

incidence so that the exciton density in K and -K valleys are the same. It is expected to see no splitting under 0T and a splitting increase as a function of B field strength by the Zeeman effect alone. From Fig.9a, the circular basis emission intersects at 0T, which aligns with the prediction. Furthermore, the result is also a demonstration of the Zeeman effect, showing that the external B field has an opposite effect on the peak energy of $\sigma\pm$ valleys (or spins). The DCP test with linear ecitation is due to thermalization, where excitons tend to stay in the lower energy valley than the other. Therefore, when B field applies, the energy difference between $\sigma\pm$-excited valley enlarges due to Zeeman effect, and exctions moves to lower energy state accordingly. Hence, the difference between $\sigma\pm$ exciton density changes with respect to the B field strength applied to the sample. In Fig.9c, the data shows as expected that the intensity of circular basis emission changes followed by B field change. In addition, Fig.9b shows that the sample has a g-factor of -13.41, which indicates the heterobilayer has a 60° degree twist angle.

To truly understand the splitting caused by imbalance, we should compare the difference in energy splitting when different incident polarization is applied. Thus, experiments are

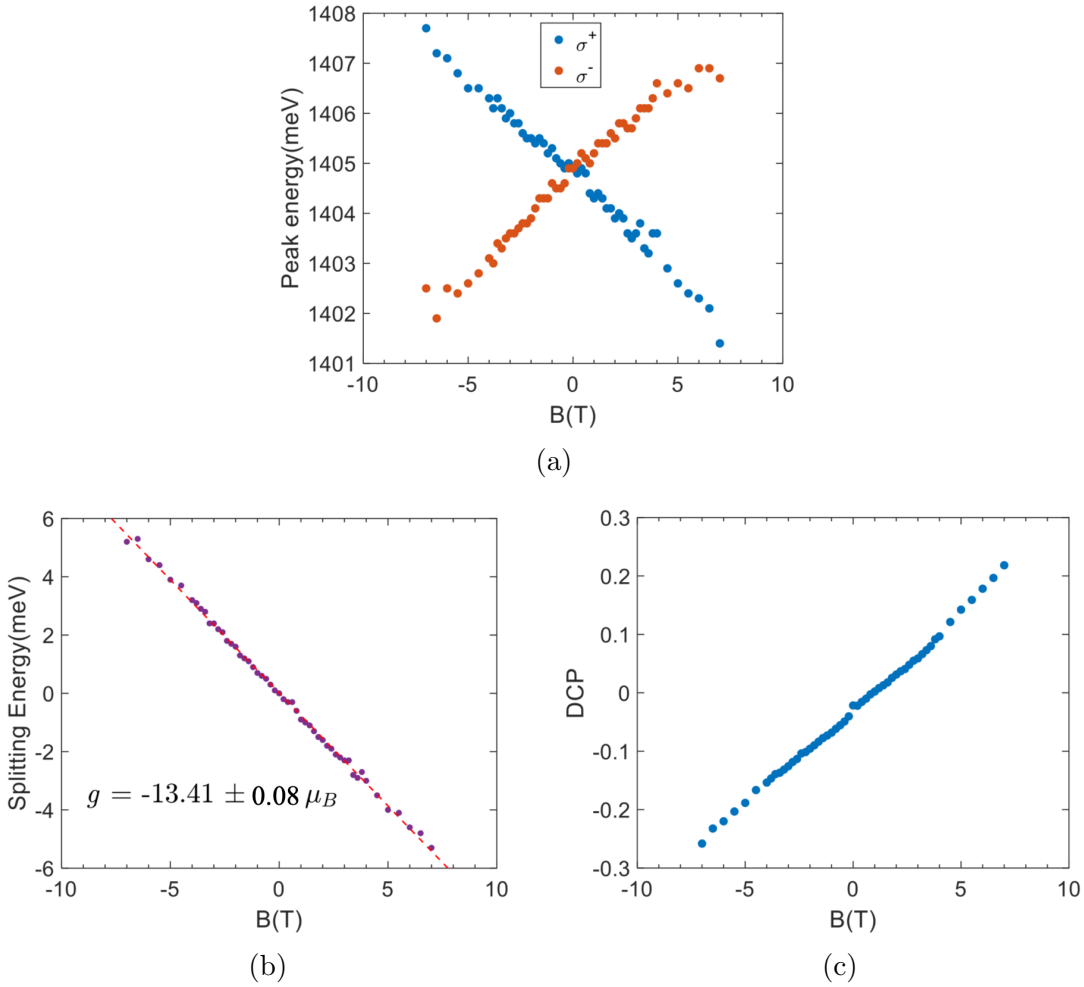

Figure 9: Linear polarized incident excitation under B field. **a**. Peak energy of interlayer excitons under $\sigma\pm$ collection. **b**. B-dependent splitting energy. The interlayer exciton exhibits g-factor close to -15, which corresponds to 60° twist angle in the sample [2]. **c**. DCP of $\sigma\pm$ peak energies under B field.

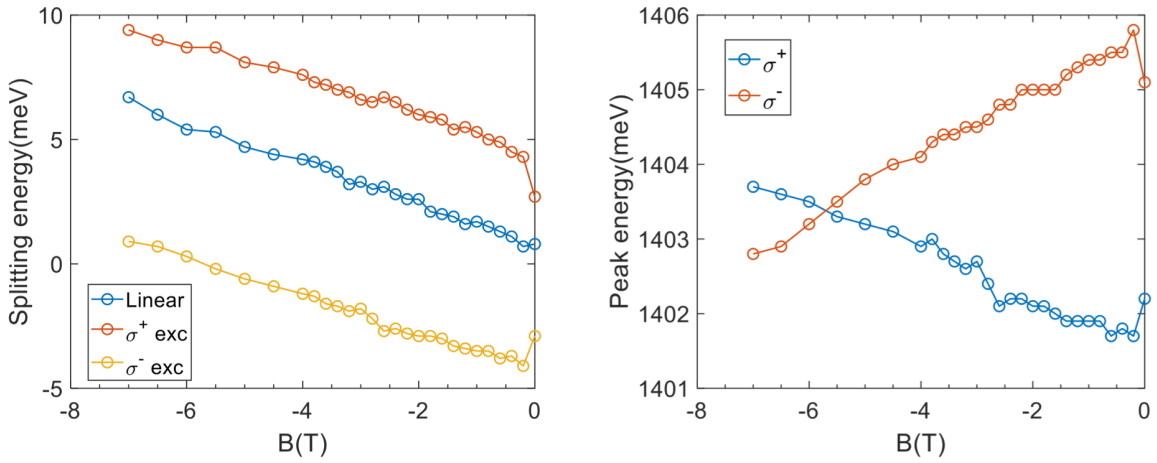

(a) (b)

Figure 10: Dependence on incident polarization under B field. **a**. B-dependent splitting energy. The splitting energy is enhanced with $\sigma+$ excitation and suppressed with $\sigma-$. **b**. Peak energy of interlayer excitons under $\sigma\pm$ collection. The effect of external B field is cancelled at around -6T.

conducted by applying linear and circular basis excitation (shown in Fig.10a). At 0T, the splitting energy with linear polarized excitation is around 0 meV as expected, but the $\sigma+$ excitation has an enhanced splitting energy and $\sigma-$ excitation an suppressed splitting energy. The data matches with our theory that the imbalance in valley species causes the splitting effect, which resembles the Zeeman splitting by adding external B field. Besides, the splitting is cancelled at -6T when excited with $\sigma-$ (shown in Fig.10b). It indicates that the optical-induced splitting at $1.5\mu W$ power has a relative same effect as Zeeman splitting at -6T when pumped but in the opposite direction. Hence, we can safely conclude that the optical-induced B field effect is as effective as the Zeeman effect by B field.

Like the Zeeman effect, the energy splitting of the optical-induced B field effect should be modulated accordingly by power pumping. The power-dependence test is conducted to check its effectiveness of the Zeeman-like splitting. When a fixed B field (B = 3T), the splitting energy is initially dominated by Zeeman effect; as power increases, the imbalance effect dominates the energy splitting.

To conclude, the imbalance caused by valley polarization creates a similar Zeeman effect

which affects oppositely on different vallleys/spins. By adding more power, we are able to create more excitons and thus larger exchange interaction energy in one valley than the other, which leads to larger splittings.

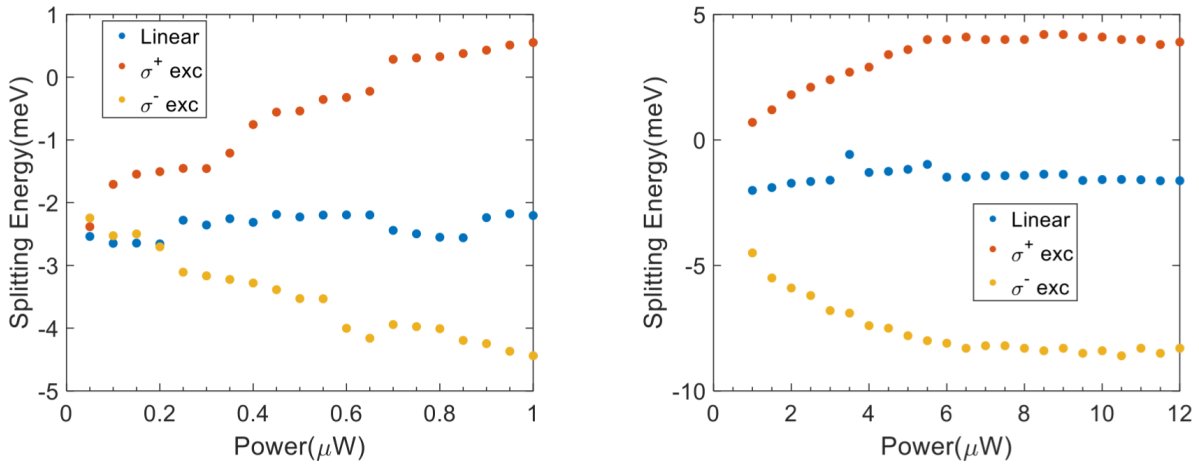

(a)

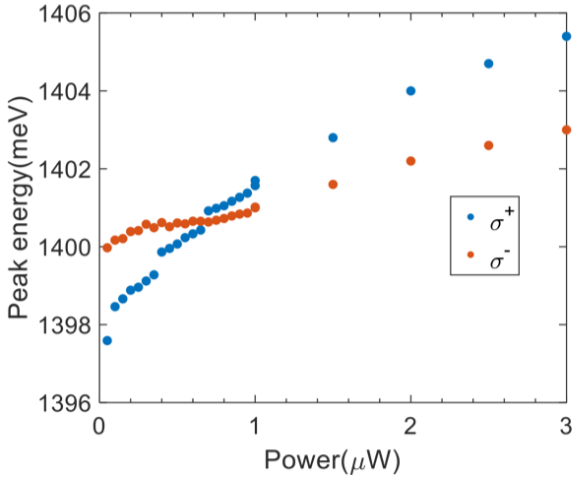

(b)

Figure 11: Power dependence test with fixed B field at 3T. **a**. B-dependent splitting energy in smaller (left) and larger (right) power range. The energy splitting is initially dominated by Zeeman effect when power is small ($0 \sim 0.2\ \mu W$), and the additional splitting is contributed by spin-valley imbalance due to polarization. **b**. Peak energy of interlayer excitons under $\sigma\pm$ collection. The effect of external B field is cancelled at the intersection point.

4 Conclusion

In summary, our results confirm with our prediction that the exchange interaction by optical excitation can induce energy splitting. Moreover, by power pumping, the largest energy splitting we can achieve is around 4 meV in the $WSe_2/MoSe_2$ system, which is equivalent to the Zeeman effect under 6T magnetic field. Hence, we can obtain a similar Zeeman splitting effect in the moiré system without applying B field instead, which provides an optical degree of freedom of energy splitting and opens up the possibilities for magneto-valleytronics applications.

5 Future Work

Many studies have discussed the possibilities of valleytronics as an alternative of electron- or spin-based semiconductor technologies since the 1970s. Vallyetronics exploits the charged particles and spin-valley degree of freedom to store and process information, which provides a new platform for quantum computing technology. One obstacle is that most of the bulk materials lack a strong coupling between the valley and external fields. Nevertheless, the emergence of 2D materials opens new doors to valleytronics for external valley-dependent fields, such as electric, magnetic, and optical fields [24].

In particular, our project focuses on valley polarization control, which allows valleytronic applications to have an additional optical knob control. Relevant work has been done regarding the effects of strain and magnetic field in the valley system [25, 26]. Our results of optical-dependent Valley Zeeman splitting provide a possible angle to the future of the valleytronic applications using an optical-induced pseudo magnetic field, which might be helpful for developing optoelectronic devices and other possible use in optical controlled ferromagnetic applications, such as non-reciprocal or one-way propagation of light without external magnetic field.

References

[1] Tran, K. *et al.* Evidence for moiré excitons in van der waals heterostructures. *Nature* **567**, 71–75 (2019).

[2] Seyler, K. L. *et al.* Signatures of moiré-trapped valley excitons in mose 2/wse 2 heterobilayers. *Nature* **567**, 66–70 (2019).

[3] Jin, C. *et al.* Observation of moiré excitons in wse 2/ws 2 heterostructure superlattices. *Nature* **567**, 76–80 (2019).

[4] Alexeev, E. M. *et al.* Resonantly hybridized excitons in moiré superlattices in van der waals heterostructures. *Nature* **567**, 81–86 (2019).

[5] Tang, Y. *et al.* Simulation of hubbard model physics in wse 2/ws 2 moiré superlattices. *Nature* **579**, 353–358 (2020).

[6] Li, W., Lu, X., Dubey, S., Devenica, L. & Srivastava, A. Dipolar interactions between field-tuneable, localized emitters in van der waals heterostructures. *arXiv preprint arXiv:1910.08139* (2019).

[7] Neto, A. C., Guinea, F., Peres, N. M., Novoselov, K. S. & Geim, A. K. The electronic properties of graphene. *Reviews of modern physics* **81**, 109 (2009).

[8] Mak, K. F. & Shan, J. Photonics and optoelectronics of 2d semiconductor transition metal dichalcogenides. *Nature Photonics* **10**, 216 (2016).

[9] Zhu, B., Chen, X. & Cui, X. Exciton binding energy of monolayer ws 2. *Scientific reports* **5**, 9218 (2015).

[10] Yu, H., Cui, X., Xu, X. & Yao, W. Valley excitons in two-dimensional semiconductors. *National Science Review* **2**, 57–70 (2015).

[11] Xiao, D., Liu, G.-B., Feng, W., Xu, X. & Yao, W. Coupled spin and valley physics in monolayers of mos 2 and other group-vi dichalcogenides. *Physical Review Letters* **108**, 196802 (2012).

[12] Schaibley, J. R. *et al.* Valleytronics in 2d materials. *Nature Reviews Materials* **1**, 16055 (2016).

[13] Rivera, P. *et al.* Valley-polarized exciton dynamics in a 2d semiconductor heterostructure. *Science* **351**, 688–691 (2016).

[14] Urbaszek, B. & Srivastava, A. Materials in flatland twist and shine (2019).

[15] Cao, Y. *et al.* Unconventional superconductivity in magic-angle graphene superlattices. *Nature* **556**, 43 (2018).

[16] Yu, H., Liu, G.-B., Tang, J., Xu, X. & Yao, W. Moiré excitons: From programmable quantum emitter arrays to spin-orbit–coupled artificial lattices. *Science advances* **3**, e1701696 (2017).

[17] Aivazian, G. *et al.* Magnetic control of valley pseudospin in monolayer wse 2. *Nature Physics* **11**, 148–152 (2015).

[18] Srivastava, A. *et al.* Valley zeeman effect in elementary optical excitations of monolayer wse_2. *Nature Physics* **11**, 141 (2015).

[19] Li, Y. *et al.* Valley splitting and polarization by the zeeman effect in monolayer $mose_2$. *Physical review letters* **113**, 266804 (2014).

[20] Rivera, P. *et al.* Observation of long-lived interlayer excitons in monolayer mose 2–wse 2 heterostructures. *Nature communications* **6**, 1–6 (2015).

[21] Chakraborty, C., Kinnischtzke, L., Goodfellow, K. M., Beams, R. & Vamivakas, A. N. Voltage-controlled quantum light from an atomically thin semiconductor. *Nature nanotechnology* **10**, 507 (2015).

[22] Yu, H., Cui, X., Xu, X. & Yao, W. Valley excitons in two-dimensional semiconductors. *National Science Review* **2**, 57–70 (2015).

[23] Hsu, W.-T. *et al.* Optically initialized robust valley-polarized holes in monolayer wse 2. *Nature communications* **6**, 1–8 (2015).

[24] Schaibley, J. R. *et al.* Valleytronics in 2d materials. *Nature Reviews Materials* **1**, 1–15 (2016).

[25] Shkolnikov, Y., De Poortere, E., Tutuc, E. & Shayegan, M. Valley splitting of alas two-dimensional electrons in a perpendicular magnetic field. *Physical review letters* **89**, 226805 (2002).

[26] Gunawan, O. *et al.* Valley susceptibility of an interacting two-dimensional electron system. *Physical review letters* **97**, 186404 (2006).